

Spectral distortions in the cosmic microwave background polarization

Sébastien Renaux-Petel,^{1,2} Christian Fidler,³ Cyril Pitrou,^{2,4} and Guido W. Pettinari⁵

¹Laboratoire de Physique Théorique et Hautes Energies, Université Pierre & Marie Curie - Paris VI, CNRS-UMR 7589, 4 place Jussieu, 75252 Paris, France

²Sorbonne Universités, Institut Lagrange de Paris, 98 bis Bd Arago, 75014 Paris, France

³Institute of Cosmology and Gravitation, Dennis Sciama Building, Burnaby Road, Portsmouth, PO1 3FX (United Kingdom)

⁴Institut d'Astrophysique de Paris, Université Pierre & Marie Curie - Paris VI, CNRS-UMR 7095, 98 bis Bd Arago, 75014 Paris, France

⁵Department of Physics & Astronomy, University of Sussex, Brighton BN1 9QH, UK

Abstract. We compute the spectral distortions of the Cosmic Microwave Background (CMB) polarization induced by non-linear effects in the Compton interactions between CMB photons and the flow of intergalactic electrons. This signal is of the y -type and is dominated by contributions arising from the reionized era. We stress that it is not shadowed by the thermal SZ effect which has no equivalent for polarization. We decompose its angular dependence into E - and B -modes, and we calculate the corresponding power spectra, both exactly and using a suitable Limber approximation that allows a simpler numerical evaluation. We find that B -modes are of the same order of magnitude as E -modes. Both spectra are relatively flat, peaking around $\ell = 280$, and their overall amplitude is directly related to the optical depth to reionization. Moreover, we find this effect to be one order of magnitude larger than the non-linear kinetic Sunyaev-Zel'dovich effect in galaxy clusters. Finally, we discuss how to improve the detectability of our signal by cross-correlating it with other quantities sourced by the flow of intergalactic electrons.

Contents

1	Introduction	1
2	Describing the spectral distortions of polarization	3
2.1	The distribution function and its spectral decomposition	3
2.2	Leading order solution of the Boltzmann equation	5
2.3	Multipolar expansion of the polarization distortion	7
3	Angular power spectra of polarization spectral distortions	8
3.1	Exact angular power spectra	8
3.2	Limber approximation	9
4	Numerical results and discussion	10
5	Conclusions	15
A	Multipolar expansion of the collision term	16
B	Correlation functions of polarization patterns and angular power spectra	17
C	Cross-correlation with intensity distortion	18
D	Expressions of special functions	21

1 Introduction

The Planck mission has recently provided exquisite maps of the temperature anisotropies of the Cosmic Microwave Background (CMB) radiation, from which angular spectra and cosmological parameters were extracted [1]; measurements of the polarized signal, especially in the E -modes, will be released soon. More generally, the CMB has been the leading probe of cosmology in the past decades, mainly because its physics is well described by linear perturbation theory, in sharp contrast with the highly non-linear dynamics of large scale structure formation, which involves density fluctuations of order unity. However, the precision of current CMB measurements is such that non-linear effects cannot be ignored anymore. For example, lensing effects by the foreground distribution of matter have to be taken into account in the angular power spectra of the CMB [2], and the lensing potential has even been reconstructed from the connected four-point correlation function of the temperature fluctuations [3]. Furthermore, the three-point correlation function has been used to provide stringent limits on primordial non-Gaussianity and to detect the correlation between the gravitational lensing and the integrated Sachs-Wolfe effect [4]. It thus becomes clear that the CMB science will now be driven by the study of non-linear effects.

In this respect, an effect that has comparatively received much less attention than the ones aforementioned is the study of the frequency dependence of the CMB. At linear level, no deviation from a blackbody spectrum is generated¹ and the spectral information is solely characterized by a direction-dependent temperature. However, in full generality, the observed CMB radiation depends non-trivially both on the direction of observation and on the energy, or frequency of the photons received. Future possible CMB experiments, such as PRISM [5] or PIXIE [6], will map the intensity and linear polarization over the full sky in many spectral channels, allowing to probe with great accuracy the deviations from a pure blackbody spectrum, or so-called spectral distortions. Besides the well-known and already observed thermal Sunyaev-Zel’dovich (tSZ) effect [7], there exists a guaranteed minimal signal, generated before recombination, within the reach of these experiments [8]. More generally, spectral distortions are a powerful probe of many physical phenomena that inject energy into the primordial plasma, such as dark matter annihilation or Silk damping of primordial density perturbations (see e.g. Refs. [8–10]).

At the non-linear level, Compton collisions also induce deviations from a pure blackbody spectrum [11] from the non-linear couplings of photons with the bulk velocity of baryons, v_b , during the reionized era. These distortions are mainly of the y -type and their angular spectrum has been computed numerically [12]. However, since distortions of this type are also generated by the tSZ effect, this signal is shadowed by the contributions coming from unresolved point sources [13]. Indeed, the thermal energy of electrons in a typical galaxy cluster, $k_B T_e$, is four orders of magnitude larger than their bulk motion kinetic energy, $m_e v_b^2/2$.

The situation is different when considering the frequency dependence of the CMB polarization, which is the topic of this paper. In this case, the tSZ effect is subdominant since it introduces only a correction of order $6k_B T_e/(m_e c^2) \sim 10^{-1}$ to the leading effect (see Eq. (36) of Ref. [14]), the latter being due to the local quadrupole of the radiation in the baryon rest frame [15–17] (note that there is also a contribution to polarization when considering effects at second order in optical depth with directional dependence like inside clusters, see § 3.3 of Ref. [18] and § 4.2 of Ref. [19]). This quadrupole can be intrinsic to the CMB as it was sourced by free-streaming since the last scattering surface, or it can be due to the local motion of baryons. However, only the second physical process, known in this context as the non-linear kinetic Sunyaev Zel’dovich (kSZ) effect [18], has a spectral dependence of the y -type [14, 19].

In this article, we consider the non-linear kSZ effect due to the bulk velocities of baryons in the intergalactic medium, and compute its unavoidable contribution to the y -type spectral distortion in polarization. We compare to previous results for the non-linear kSZ effect generated by clusters [17], and find that the intergalactic contribution is one order of magnitude larger.

The outline of the paper is as follows. In § 2, we first present the description of spectral distortions of the y -type in the linearly polarized CMB. We then discuss the dynamics of such type of distortion from the Boltzmann equation, and derive the general solution for the angular multipoles of the E - and B -modes of distortions. In § 3, we obtain the exact expression for

¹In the absence of phenomena that inject energy into the primordial plasma.

their angular power spectra, and present a suitable Limber approximation. We finally present numerical results in § 4, both with the exact and approximate methods, and discuss our results. We conclude in § 5 and gather some technical details in four appendices.

2 Describing the spectral distortions of polarization

2.1 The distribution function and its spectral decomposition

In this section, we introduce our set-up and notations, following Ref. [20] to which we refer the reader for more details. The description of polarized radiation is formulated by introducing a field of tetrad basis, *i.e.* a set of four vector fields $e_{(a)}^\mu$ ($a = 0, 1, 2, 3$) that satisfy

$$\eta_{(a)(b)} = g_{\mu\nu} e_{(a)}^\mu e_{(b)}^\nu, \quad g_{\mu\nu} = \eta_{(a)(b)} e_{(a)}^\mu e_{(b)}^\nu \quad (2.1)$$

where $g_{\mu\nu}$ is the spacetime metric and $\eta_{(a)(b)}$ is the Minkowski metric. This defines everywhere a local frame which is used to separate the magnitude of the photon momentum from its direction [21]. We project the photon momentum p^μ onto the set of tetrads, using $p^\mu = p^{(a)} e_{(a)}^\mu$, and further define the comoving momentum q and the photon direction $n^{(i)}$ as

$$p^{(0)} = \frac{q}{a}, \quad p^{(i)} = \frac{q}{a} n^{(i)} \quad (i = 1, 2, 3) \quad (2.2)$$

where $n_{(i)} n^{(i)} = 1$ and a is the cosmological scale factor. Physically, with the choice $e^{(0)} \propto d\eta$ where η denotes conformal time, the above q is simply proportional to the energy measured by an observer whose worldline is orthogonal to constant time hypersurfaces: $q = aE_{\text{phys}}$.

To describe the polarized radiation in the statistical description, one has to introduce a Hermitian tensor-valued distribution function, $f_{\mu\nu}(\eta, \mathbf{x}, p^{(i)})$, such that

$$\epsilon^\mu \epsilon^{*\nu} f_{\mu\nu}(\eta, \mathbf{x}, p^{(i)}) \quad (2.3)$$

is the number density in phase space of photons at $(\eta, \mathbf{x}, p^{(i)})$ with polarization state vector ϵ^μ (see Refs. [21, 22] and references therein). We also define the direction 4-vector of photons n^μ by $n^\mu \equiv n^{(i)} e_{(i)}^\mu$, with which we define the projection operator, also often called the screen projector, as

$$S_{\mu\nu} \equiv g_{\mu\nu} + e^{(0)}_\mu e^{(0)}_\nu - n_\mu n_\nu. \quad (2.4)$$

By definition, $S_{\mu\nu}$ is a projector onto the two dimensional hypersurface orthogonal to both $e^{(0)}_\mu$ and n_μ , that is, the plane on which “lives” the complex-valued and Hermitian distribution function $f_{\mu\nu}$ describing the polarization of radiation². The latter can be decomposed, in the absence of circular polarization - as relevant in the standard cosmological context - as³

$$f_{\mu\nu} \equiv \frac{1}{2} (I S_{\mu\nu} + P_{\mu\nu}), \quad (2.5)$$

²The distribution function verifies indeed $f_{\mu\nu} = S_\mu^\alpha S_\nu^\beta f_{\alpha\beta}$. See e.g. Refs. [20, 23] for more details.

³Note that the $P_{\mu\nu}$ defined in this paper is equal to $2P_{\mu\nu}$ of Refs. [20, 23].

where I is the intensity and the symmetric traceless tensor $P_{\mu\nu}$ encodes the two degrees of linear polarization, which are parametrized by the Q and U Stokes parameters, see § 3.

On the background Friedmann-Lemaître-Robertson-Walker (FLRW) space-time, the distribution function is characterized solely by the intensity I , which follows a Planck distribution whose temperature \bar{T} depends only on time η due to the symmetries of the FLRW universe. From the background Boltzmann equation, it is easily found that $\bar{T}(\eta) = T_0 a_0/a(\eta)$ where a_0 and T_0 are respectively the scale factor and the background temperature today, so that, on the background, the intensity of the photons is described by a redshifted blackbody distribution,

$$\bar{I}(\eta, q) = I_{\text{BB}}\left(\frac{q}{a(\eta)\bar{T}(\eta)}\right) = I_{\text{BB}}\left(\frac{q}{a_0 T_0}\right), \quad \text{with } I_{\text{BB}}(x) \equiv \frac{2}{(e^x - 1)}. \quad (2.6)$$

No spectral distortion is generated at first order in perturbation theory [24], under which approximation the intensity fluctuation can simply be described by a temperature fluctuation independent of the energy q . However, Compton scattering does induce spectral distortions at second order [25, 26], which can be described by introducing the so-called y Compton parameter, entering into the Fokker-Planck expansion of the distribution function [11] as

$$\begin{aligned} I(q, n^{(i)}) &\simeq I_{\text{BB}}\left(\frac{q}{aT(n^{(i)})}\right) + y(n^{(i)}) q^{-3} \frac{\partial}{\partial \ln q} \left[q^3 \frac{\partial}{\partial \ln q} I_{\text{BB}}\left(\frac{q}{aT(n^{(i)})}\right) \right] \\ &= I_{\text{BB}}\left(\frac{q}{aT(n^{(i)})}\right) + y(n^{(i)}) \mathcal{D}_q^2 I_{\text{BB}}\left(\frac{q}{aT(n^{(i)})}\right), \end{aligned} \quad (2.7)$$

where

$$\mathcal{D}_q^2 \equiv q^{-3} \frac{\partial}{\partial \ln q} \left(q^3 \frac{\partial}{\partial \ln q} \right) = \frac{\partial^2}{\partial \ln q^2} + 3 \frac{\partial}{\partial \ln q} \quad (2.8)$$

and, for brevity, we have omitted the dependence of all quantities on the spacetime coordinates x^μ . The only quantities in the expansion that depend on the propagation direction of the photon are the Compton parameter y and the temperature T . This expansion is particularly convenient to describe spectral distortions. Indeed, as the number density of photon is given by $n \propto a^{-3} \int I q^2 dq$, the y term does not contribute to the photon number density and the temperature T is the temperature of the blackbody that would have the same number density.

Similarly, the spectral dependence of the polarization tensor can be split into a standard component $\mathcal{P}_{\mu\nu}$, and a spectral distortion component $y_{\mu\nu}$ as [11, 20]

$$P_{\mu\nu}(q, n^{(i)}) \simeq -\mathcal{P}_{\mu\nu}(n^{(i)}) \frac{\partial}{\partial \ln q} I_{\text{BB}}\left(\frac{q}{aT(n^{(i)})}\right) + y_{\mu\nu}(n^{(i)}) \mathcal{D}_q^2 I_{\text{BB}}\left(\frac{q}{aT(n^{(i)})}\right). \quad (2.9)$$

Note that this splitting is slightly different from the case of the intensity as there is no polarization on the background and hence no term corresponding to the first one in Eq. (2.7). Similarly to the y parameter, it can be shown that Compton scattering generates a non-vanishing $y_{\mu\nu}$ only beyond first-order perturbation theory [20]. We name this term *y-type distortion of linear polarization* or polarization distortion for short. The component $\mathcal{P}_{\mu\nu}$, on the other hand, describes the standard

polarization [27]. Let us stress eventually that the temperature T entering into Eqs. (2.7)-(2.9) is a local quantity, which can itself be expanded around the background temperature as

$$T(\eta, n^{(i)}) \equiv \bar{T}(\eta) \left[1 + \Theta(n^{(i)}) \right]. \quad (2.10)$$

2.2 Leading order solution of the Boltzmann equation

The time evolution of the distribution function $f_{\mu\nu}$ is governed by the Boltzmann equation. Since the metric fluctuations affect the energy of photons in the same proportions through free streaming, that is they affect $\ln q$ and not q , and given the parameterizations (2.7) and (2.9) which are based on logarithmic derivatives of I_{BB} , then the Boltzmann equation can be separated into dynamical equations for its spectral components Θ and y for the intensity part, or $\mathcal{P}_{\mu\nu}$ and $y_{\mu\nu}$ for the polarized part, which couple only through the collision term. More details of this procedure can be found in Refs. [11, 20, 28]. By expanding the Boltzmann equation at second order in perturbation theory, one can thus obtain the evolution equation for our quantity of interest $y_{\mu\nu}$. In the tetrad basis, it can be written in the form

$$y'_{(i)(j)} + n^{(l)} \partial_l y_{(i)(j)} = \tau' \left(-y_{(i)(j)} + C_{(i)(j)}^y \right), \quad (2.11)$$

where a prime denotes derivation with respect to the conformal time η . The Thomson interaction rate is given by $\tau' \equiv a \bar{n}_e \sigma_{\text{T}}$, where \bar{n}_e is the background density of free electrons and σ_{T} is the Thomson scattering cross section. The explicit and lengthy expression of the collision term $C_{(i)(j)}^y$ can be found in Ref. [20]. Fortunately, we do not need its full expression as the leading order term can be easily identified as

$$C_{(i)(j)}^{y(\text{L.O.})} = -\frac{1}{10} [v_{(i)} v_{(j)}]^{\text{TT}} \quad (2.12)$$

where $v_{(i)}$ is the difference between the first-order baryon velocity v_b and photon velocity v_r in the tetrad basis (in the following we shall simply refer to $v_{(i)}$ as the baryon velocity), and where TT denotes the traceless screen-projected part

$$[v_{(i)} v_{(j)}]^{\text{TT}} \equiv \left[S_{(i)}^{(k)} S_{(j)}^{(l)} - \frac{1}{2} S^{(k)(l)} S_{(i)(j)} \right] v_{(k)} v_{(l)}. \quad (2.13)$$

Although the collision term (2.12) resembles the one derived in Refs. [14–17, 19] for the overall numerical factor and the baryons velocity geometric contribution $[v_{(i)} v_{(j)}]^{\text{TT}}$, its spectral dependence is different. In our case the spectral dependence is implied by the definition (2.9) and is $\mathcal{D}_q^2 I_{\text{BB}}$, which corresponds only to spectral distortions. In these initial references, the spectral dependence of the collision term is $(\mathcal{D}_q^2 - 4\partial/\partial \ln q) I_{\text{BB}}$ and it corresponds to the total collision term, encompassing both the contributions to the spectral distortion $y_{\mu\nu}$ and the standard component $\mathcal{P}_{\mu\nu}$. After integration over the spectral dependence, this leads to the collision term for the brightness of the polarized signal (the one presented in Ref. [15]), which still possesses the geometrical dependence $[v_{(i)} v_{(j)}]^{\text{TT}}$ but then has a different numerical factor as it corresponds to the collision term of a variable proportional to $\mathcal{P}_{\mu\nu} + y_{\mu\nu}$ in our framework.

The other terms in $C_{(i)(j)}^y$ involve quantities such as the temperature fluctuations Θ , the Compton parameter y and the polarization tensor $\mathcal{P}_{\mu\nu}$. Because metric and photon perturbations do not grow, these quantities remain of the same order of the primordial potential Φ throughout the cosmic evolution. On the other hand, the baryon velocity $v_{(i)}$ after recombination ($\eta \gtrsim 280\text{Mpc}$) grows like $(k\eta)\Phi$, as shown in Fig. 1. As a result, when the baryons and the photons interact again during the era of reionization ($\eta \gtrsim 5000\text{Mpc}$), the v^2 term in (2.12) dominates over all the others in the collision term, which can therefore be safely neglected. Furthermore, we can ignore the contribution from $C_{(i)(j)}^{y(\text{L.O.})}$ coming from the time of recombination, because it was then suppressed by the tight-coupling between photons and baryons by a factor $\propto k/\tau'$ [30–33]. We remark that these assumptions were numerically demonstrated in Ref. [12] in the similar context of the intensity spectral distortion, where the contribution from recombination was shown to be suppressed by a factor $\mathcal{O}(10^2)$ compared to that from reionization.

Let us notice that because the distortion of polarization is, within our leading-order approximation, sourced only by quantities quadratic in first order perturbation theory, the tetrad basis can be considered for practical purposes to be calculated on the unperturbed background space-time. From now on we will therefore omit the parentheses in $y_{(i)(j)}$ and the likes and consider the indices $i, j \dots$ as trivial spatial comoving indices.

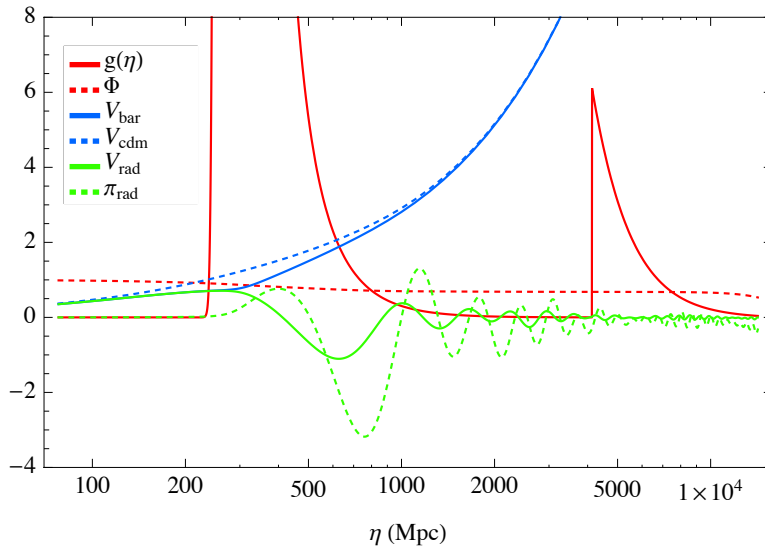


Figure 1. Red continuous line: visibility function (2.22) (magnified by a factor 10^5) for a model of instantaneous reionization. Red dashed line: scalar gravitational potential (set to unity deep in the radiation era). Blue continuous line: scalar part of baryon velocity. Blue dashed line: scalar part of cold dark matter velocity. Green continuous line: scalar part of photons velocity. Green dashed line: scalar part of radiation anisotropic stress. All contributions are evaluated for the Fourier mode $k = 0.01 \text{ Mpc}^{-1}$.

In order to numerically compute the spectral distortion y_{ij} , we make use of the line of sight

solution of the Boltzmann equation [34], which for (2.11) and in Fourier space formally reads⁴

$$y_{ij}(\eta_0, k_i, n^i) = \int_{\eta_{\text{re}}}^{\eta_0} d\eta \tau' e^{-\tau} e^{-i k_i n^i r(\eta)} C_{ij}^y(\eta, k_i, n^i) \quad (2.14)$$

where $d\tau(\eta)/d\eta \equiv -\tau'$, $\tau(\eta_0) = 0$, $r(\eta) \equiv \eta_0 - \eta$ is the comoving distance from us, η_0 is the present conformal time and η_{re} denotes a time slightly before the beginning of reionization. At leading order, replacing C_{ij}^y by $C_{ij}^{y(\text{L.O.})}$ in Eq. (2.14) provides an explicit integral solution once the first-order velocity v_i is known.

2.3 Multipolar expansion of the polarization distortion

We now proceed to a multipolar expansion of the distortion tensor $y_{ij}(\mathbf{k}, \hat{\mathbf{n}})$ (we omit the mention of η_0 from now on without ambiguity). We choose the z axis along the direction of the Fourier vector \mathbf{k} of interest. The traceless projected tensor $y_{ij}(\mathbf{k}, \hat{\mathbf{n}})$ can then be expanded on the natural polarization basis m_i^\pm as [29, 35]

$$y_{ij}(\mathbf{k}, \hat{\mathbf{n}}) = \sum_{\pm} \sum_{\ell=2}^{\infty} \sum_{m=-\ell}^{\ell} [E_{\ell m}^y(\mathbf{k}) \pm i B_{\ell m}^y(\mathbf{k})] \frac{Y_{\ell m}^{\pm 2}(\hat{\mathbf{n}})}{N_{\ell}} m_i^{\pm} m_j^{\pm} \quad (2.15)$$

where $N_{\ell} \equiv i^{\ell} \sqrt{(2\ell+1)/(4\pi)}$, $m_i^{\pm} \equiv (\hat{e}_i^{\theta} \mp i \hat{e}_i^{\phi})/\sqrt{2}$ with standard spherical coordinates, and where a hat on a vector indicates that it is of unit norm.

As for v_i sourcing y_{ij} , it only contains a scalar mode in the standard cosmological model and reads

$$v_i(\eta, \mathbf{k}) = -i \hat{k}_i F(k, \eta) \Phi(\mathbf{k}) \quad (2.16)$$

where $\Phi(\mathbf{k})$ is the primordial gravitational potential and $F(k, \eta)$ denotes the transfer function of the baryon velocity. From this, one can arrive at the multipolar decomposition of the leading order collision term (see Appendix A for the derivation):

$$C_{ij}^{y(\text{L.O.})}(\eta, \mathbf{k}, \hat{\mathbf{n}}) = \sum_{\ell, m, \pm} E[C^y]_{\ell m}(\mathbf{k}) \frac{Y_{\ell m}^{\pm 2}(\hat{\mathbf{n}})}{N_{\ell}} m_i^{\pm} m_j^{\pm} \quad (2.17)$$

where

$$E[C^y]_{\ell m}(\mathbf{k}) = \delta_{\ell}^2 \mathcal{K} \left\{ S_m(\hat{\mathbf{k}}_1, \hat{\mathbf{k}}_2) F(k_1, \eta) F(k_2, \eta) \Phi(k_1) \Phi(k_2) \right\} \quad (2.18)$$

and where

$$\mathcal{K}\{\dots\} \equiv \int \frac{d^3 \mathbf{k}_1 d^3 \mathbf{k}_2}{(2\pi)^3} \delta_{\text{D}}^3(\mathbf{k}_1 + \mathbf{k}_2 - \mathbf{k}) \dots \quad (2.19)$$

denotes the convolution operator. The expression of the geometrical factor $S_m(\hat{\mathbf{k}}_1, \hat{\mathbf{k}}_2)$ can be found in Eq. (A.11).

⁴Our convention for the Fourier transformation is such that for every real-space quantity $A(\mathbf{x})$, we define its Fourier transform as $A(\mathbf{k}) = \int d^3 \mathbf{x} e^{-i \mathbf{k} \cdot \mathbf{x}} A(\mathbf{x})$.

Similarly to the case of the standard polarization, the (leading-order) collision term from Thomson scattering only contains an electric part, *i.e.* the magnetic part $B[C^y]_{\ell m}$ vanishes identically. However, free-streaming does produce an observable magnetic pattern in the polarization distortion out of the pure E -modes from the collision term. This can be seen by inserting Eq. (2.17) into the expression (2.14) and by using the Rayleigh formula to expand $e^{-ik_i n^i r}$ into spherical harmonics. The rules for the addition of spherical harmonics can then be used to obtain expressions for the electric and magnetic parts of the distortion tensor y_{ij} analogous to the ones of the standard polarization [35]:

$$\frac{E_{\ell m}^y(\mathbf{k})}{2\ell + 1} = \mathcal{K} \left\{ \int_{\eta_{\text{re}}}^{\eta_0} d\eta g(\eta) \epsilon_{\ell}^{(m)}[kr(\eta)] S_m(\hat{\mathbf{k}}_1, \hat{\mathbf{k}}_2) F(k_1, \eta) F(k_2, \eta) \Phi(k_1) \Phi(k_2) \right\} \quad (2.20)$$

$$\frac{B_{\ell m}^y(\mathbf{k})}{2\ell + 1} = \mathcal{K} \left\{ \int_{\eta_{\text{re}}}^{\eta_0} d\eta g(\eta) \beta_{\ell}^{(m)}[kr(\eta)] S_m(\hat{\mathbf{k}}_1, \hat{\mathbf{k}}_2) F(k_1, \eta) F(k_2, \eta) \Phi(k_1) \Phi(k_2) \right\} \quad (2.21)$$

where we defined the visibility function

$$g(\eta) = \tau' e^{-\tau}. \quad (2.22)$$

The explicit expressions of the projection functions $\epsilon_{\ell}^{(m)}$ and $\beta_{\ell}^{(m)}$ are reported for completeness in Appendix D.

3 Angular power spectra of polarization spectral distortions

In the previous section we have defined the multipolar decomposition Eq. (2.15) of the Fourier components of the distortion tensor y_{ij} and obtained the explicit expressions Eqs. (2.20)-(2.21) of its electric and magnetic parts. In this section, we relate these quantities to correlation functions of real-space observables.

3.1 Exact angular power spectra

Out of the distortion tensor, one can extract the distortion Stokes parameters Q^y and U^y defined as

$$y_{ij}(\mathbf{x}, \hat{\mathbf{n}}) = \sum_{\pm} (Q^y \pm iU^y)(\mathbf{x}, \hat{\mathbf{n}}) m_i^{\pm} m_j^{\pm}. \quad (3.1)$$

The latter can be decomposed onto spherical harmonics as

$$(Q^y \pm iU^y)(\mathbf{x}, \hat{\mathbf{n}}) = \sum_{\ell=2}^{\infty} \sum_{m=-\ell}^{\ell} (e_{\ell m}^y(\mathbf{x}) \pm i b_{\ell m}^y(\mathbf{x})) Y_{\ell m}^{\pm 2}(\hat{\mathbf{n}}; \hat{\mathbf{e}}) \quad (3.2)$$

where in $Y_{\ell m}^{\pm 2}(\hat{\mathbf{n}}; \hat{\mathbf{e}})$ we have made it explicit that the spin-2 spherical harmonic is defined with respect to an (arbitrary) real-space axis $\hat{\mathbf{e}}$, contrary to the previous section in which this axis

was aligned with the Fourier wavevector of interest. We then define the angular power spectra as

$$C_\ell^{E^y} \equiv \langle |e_{\ell m}^y(\mathbf{x})|^2 \rangle \quad \text{and} \quad C_\ell^{B^y} \equiv \langle |b_{\ell m}^y(\mathbf{x})|^2 \rangle. \quad (3.3)$$

We do not consider the cross-correlation $\langle e_{\ell m}^y(\mathbf{x}) b_{\ell' m'}^{y*}(\mathbf{x}) \rangle$ because it vanishes by parity conservation. In Appendix B, we give the relations between these power-spectra and angular correlation functions of spin-0 quantities built out of Q^y and U^y .

Following standard calculations for the polarization, such as in Refs. [35, 36], the power spectra can be expressed as

$$(2\ell + 1)^2 C_\ell^{E^y} = \frac{2}{\pi} \sum_{m=-2}^2 \int dk k^2 \mathcal{Q}_{\ell m}^{E^y}(k), \quad (3.4)$$

and similarly for $C_\ell^{B^y}$, where we defined

$$\langle E_{\ell m}^y(\mathbf{k}) E_{\ell' m'}^{y*}(\mathbf{k}') \rangle = (2\pi)^3 \delta_D^3(\mathbf{k} - \mathbf{k}') \mathcal{Q}_{\ell m}^{E^y}(k) \delta_{mm'}. \quad (3.5)$$

The crucial difference between our set-up and the one of the standard polarization is that in the latter case, $E_{\ell m}$ and $B_{\ell m}$ are linear in the Gaussian variable Φ whereas $E_{\ell m}^y$ and $B_{\ell m}^y$ in Eqs. (2.20)-(2.21) are quadratic in the primordial potential Φ , and hence involve a convolution operator. Using Wick theorem, one can find the following expressions:

$$\mathcal{Q}_{\ell m}^{E^y}(k) = \frac{2(2\ell + 1)^2}{(2\pi)^3} \int d^3 \mathbf{k}_1 P(k_1) P(k_2) \left| S_m(\hat{\mathbf{k}}_1, \hat{\mathbf{k}}_2) \right|^2 \left| \int_{\eta_{\text{re}}}^{\eta_0} d\eta g(\eta) \epsilon_\ell^{(m)}[kr(\eta)] F(k_1, \eta) F(k_2, \eta) \right|^2 \quad (3.6)$$

$$\mathcal{Q}_{\ell m}^{B^y}(k) = \frac{2(2\ell + 1)^2}{(2\pi)^3} \int d^3 \mathbf{k}_1 P(k_1) P(k_2) \left| S_m(\hat{\mathbf{k}}_1, \hat{\mathbf{k}}_2) \right|^2 \left| \int_{\eta_{\text{re}}}^{\eta_0} d\eta g(\eta) \beta_\ell^{(m)}[kr(\eta)] F(k_1, \eta) F(k_2, \eta) \right|^2 \quad (3.7)$$

where $P(k)$ is the primordial power spectrum of the potential Φ , defined as

$$\langle \Phi(\mathbf{k}) \Phi^*(\mathbf{k}') \rangle = (2\pi)^3 \delta_D^3(\mathbf{k} - \mathbf{k}') P(k), \quad (3.8)$$

and where it is understood that $\mathbf{k}_2 = \mathbf{k} - \mathbf{k}_1$. Because of statistical isotropy, the integrands in Eqs. (3.6)-(3.7) do not depend on the azimuthal angle of \mathbf{k}_1 around \mathbf{k} . Therefore the Fourier integrals there are only truly two-dimensional, that is, $d^3 \mathbf{k}_1 = 2\pi k_1^2 dk_1 \sin \theta_{\mathbf{k}_1} d\theta_{\mathbf{k}_1}$, where $\theta_{\mathbf{k}_1}$ denotes the angle between \mathbf{k}_1 and \mathbf{k} . Let us note eventually that $\mathcal{Q}_{\ell, -1}^{E^y} = \mathcal{Q}_{\ell, 1}^{E^y}$ and $\mathcal{Q}_{\ell, -2}^{E^y} = \mathcal{Q}_{\ell, 2}^{E^y}$. For this reason, we simply call in the following the $m = 1$ contribution to the spectra the sum of the $m = -1$ and $m = 1$ contributions (and similarly for $m = 2$).

3.2 Limber approximation

In the small scale limit, one can simplify the exact results in Eqs. (3.4)-(3.6)-(3.7) by using the Limber approximation [37] (see also Refs. [38, 39]). Noting that the functions $\epsilon_\ell^{(m)}$ and $\beta_\ell^{(m)}$ are

built out of the spherical Bessel functions j_ℓ and their derivatives (see Appendix D), and using that for a slowly varying function with respect to the oscillations of the j_ℓ 's,

$$\int_0^\infty f(x) j_\ell(x) dx = \sqrt{\frac{\pi}{2\nu}} f(\nu) + \mathcal{O}\left(\frac{1}{\nu^2}\right), \quad (3.9)$$

where $\nu = \ell + \frac{1}{2}$, one obtains the leading-order results

$$C_{\ell \text{ Limber}}^{E^y} = \frac{1}{4(2\pi)^2} \int_0^{r_{\text{re}}} \frac{dr}{r^2} k_1^2 dk_1 \sin \theta_{\mathbf{k}_1} d\theta_{\mathbf{k}_1} P(k_1) P(k_2) [g(\eta) F(k_1, \eta) F(k_2, \eta)]^2 \\ \times \left(3 |S_0(\hat{\mathbf{k}}_1, \hat{\mathbf{k}}_2)|^2 + |S_2(\hat{\mathbf{k}}_1, \hat{\mathbf{k}}_2)|^2 \right) \quad (3.10)$$

and

$$C_{\ell \text{ Limber}}^{B^y} = \frac{1}{(2\pi)^2} \int_0^{r_{\text{re}}} \frac{dr}{r^2} k_1^2 dk_1 \sin \theta_{\mathbf{k}_1} d\theta_{\mathbf{k}_1} P(k_1) P(k_2) [g(\eta) F(k_1, \eta) F(k_2, \eta)]^2 |S_1(\hat{\mathbf{k}}_1, \hat{\mathbf{k}}_2)|^2 \quad (3.11)$$

where $\mathbf{k}_2 = \mathbf{k} - \mathbf{k}_1$, $kr = \ell + \frac{1}{2}$ and $\eta = \eta_0 - r$. Note that within this approximation, modes with $m = \pm 1$ (respectively with $m = 0$ and $m = \pm 2$) do not contribute to $C_{\ell}^{E^y}$ (respectively to $C_{\ell}^{B^y}$). We will see in the next subsection that the above formulae, which are numerically much easier to evaluate than the exact results, do indeed provide an excellent approximation for $\ell \gtrsim 10$.

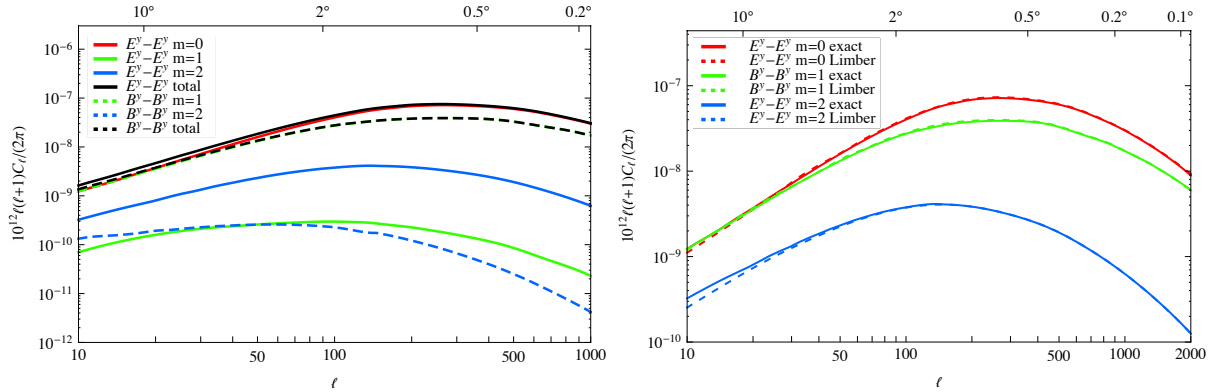


Figure 2. *Left.* Continuous black line: total E^y -modes spectrum; dashed black line: total B^y -modes spectrum. Individual contribution to the E^y -modes for $m = 0, 1, 2$ are respectively in red, green and blue continuous lines. Individual contributions to B^y -modes for $m = 1, 2$ are respectively in green and blue dashed lines. *Right.* We compare the exact spectra to their Limber approximations. Red: $m = 0$ contribution; exact formula in continuous line and Limber approximation in dashed line for E^y -modes spectrum. Green: $m = 1$ contribution; exact formula in continuous line and Limber approximation in dashed line for B^y -modes spectrum. Blue: $m = 2$ contribution; exact formula in continuous line and Limber approximation in dashed line for E^y -modes spectrum.

4 Numerical results and discussion

We compute the power spectra of the polarization distortion E^y - and B^y -modes by numerically evaluating the integrals in Eqs. (3.4)-(3.6)-(3.7) with the second-order Boltzmann code SONG [40,

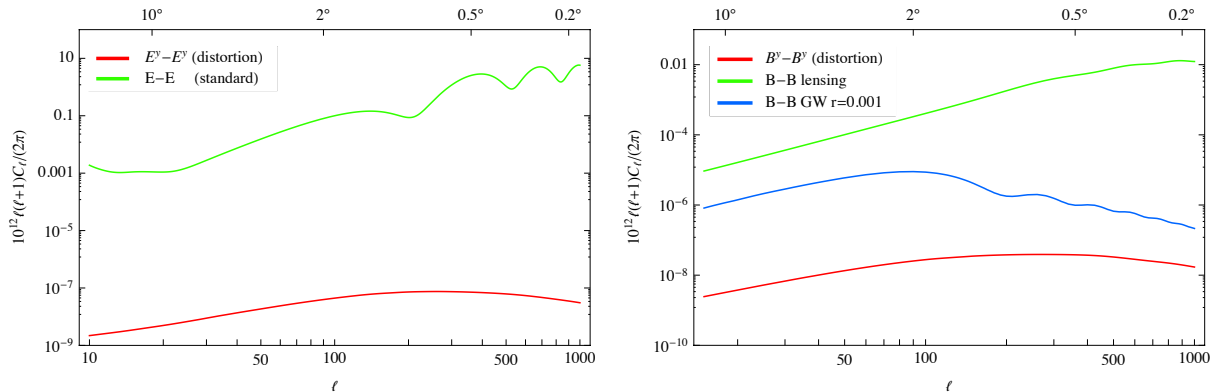


Figure 3. *Left.* Red: the E^y -modes spectrum of the y -type distortion (this article) compared to the standard E -mode polarization spectrum (green). *Right.* The B^y -modes spectrum of the y -type distortion (this article) in red compared to the standard B -modes spectrum induced by weak lensing (in green) and induced by primordial gravitational waves with tensor to scalar ratio $r = 0.001$ (in blue).

41] (Second Order Non-Gaussianity), using Planck cosmological parameters [1]. Unless otherwise stated, we consider a simple model of instantaneous reionization (see Fig. 1). We quantify the effects of an extended period of reionization in the last paragraph.

Signal of polarization distortion from reionization In the left panel of Fig. 2, we plot the total power spectra for the E^y - and B^y -modes together with their individual contributions $m = 0, 1, 2$. On the right panel, we compare the Limber approximations to the exact formulas, and see that the agreement is excellent, with the error going as $1/\ell$. The B^y -modes are of the same order of magnitude as the E^y -modes, since the sources are the same apart from geometrical factors. The signal is very smooth with no baryon acoustic oscillation structure since the baryon velocity is almost completely similar to the dark matter velocity during reionization (see Fig. 1). It peaks around $\ell = 280$, with $\ell(\ell + 1)C_\ell/(2\pi) \simeq 7 \cdot 10^{-20}$, its amplitude being controlled by the optical depth to reionization. When compared with the cluster contribution reported in Ref. [17], it is one order of magnitude larger at this scale. This can be understood from simple arguments. First, the local velocities of baryons in the intergalactic medium or of the point sources such as galaxy clusters are expected to be of the same order. Second, it is true that the baryon density is higher inside clusters due to the non-linear collapse of matter. However, when averaged at a given redshift over a volume of typical size larger than the typical intercluster scale, the number of electrons should be of the same order as the one found from the linear description. Provided we consider angular scales subtending transverse distances that are larger than the typical intercluster scale, we thus expect the contribution from the intergalactic medium computed in our mildly non-linear formalism (that is second order) to account correctly for the contribution due to the kinetic motion of clusters. With a typical intercluster distance of 20 Mpc, seen at a redshift $z = 1$, that is at a comoving distance of approximately 3400 Mpc, it corresponds to angular scales larger than $20'$, that is to multipoles ℓ smaller than roughly 500. Finally, one should however take into account the fact that the contribution from the intergalactic medium

develops from the beginning of reionization (around $z = 12$) onwards — when its contribution is the largest — whereas the contribution coming from the galaxy clusters peculiar velocity starts to contribute at much later times, when galaxy clusters have formed. Hence, the total contribution integrated over all redshifts of the intergalactic medium computed with second-order perturbation theory should be larger than the clusters contribution, at least in the range where the mildly non-linear description accounts correctly for the clusters contribution, that is for $\ell \lesssim 500$.

Finally, note that our results are in agreement with the ones of Hu in Ref. [15], who performed a similar calculation within the Limber approximation. Let us remark however that, as we have explained in § 2.2, this reference considers the brightness of the polarized signal by integrating over its spectral dependence. On the contrary, the polarization tensor is separated here between a standard component and a proper spectral distortion component [see Eq. (2.9)], that future observations have the potential to disentangle.

Comparison with the standard polarization In Fig. 3 we also compare the power spectra of the E^y - and B^y -modes of the y -type distortion with the spectra of the standard E - and B -modes of polarization. Since the y -type polarization distortion is a second-order effect, its power spectrum is expected to be much smaller than the standard polarization, as it involves two powers of the primordial power spectrum. The latter being of order 10^{-10} , one would expect the spectrum of the E^y -modes to be roughly 10 order of magnitude smaller than the one of the standard E -modes. One could even think it would be 12 orders of magnitude smaller if we take into account the fact that only 10% of the visibility function $g(\eta)$ contribute in the reionization era. However, one should take into account the facts that *i*) the standard E -modes are already suppressed by tight-coupling during recombination and *ii*) the sources (2.12) are quadratic in the linear baryon velocity, which in turn is boosted by a factor $k\eta$ with respect to the primordial fluctuations (see Fig. 1). We find indeed that the spectrum of the polarization distortion E^y -modes is approximately only 6 orders of magnitude smaller than the one of the standard E -modes at $\ell = 200$. Furthermore, the spectrum of the polarization distortion B^y -modes is two orders of magnitude smaller than the contribution from primordial gravitational waves with tensor to scalar ratio $r = 0.001$. However, one should remember that the spectral shape in the y -type polarization distortion signal is very different from the standard polarization, and that there is more signal in the former than in the latter. This can be seen from the left panel of Fig. 5, where we show the different spectral shapes of polarization, namely the standard signal and the y -type distortion, together with a blackbody spectrum for comparison. The brightness for the y -type distortion peaks at higher frequency than the brightness of the standard signal, and for nearly all frequencies it is larger in absolute value.

Improving the detectability with cross-correlations To improve the hopes of detection of the y -type polarization distortion, one can consider its cross-correlation with the y -type intensity distortion, the latter being larger in magnitude [12] and with more signal-to-noise. One might be concerned that the intensity y -type distortion is not dominated by the contribution from the non-linear kSZ effect of the intergalactic medium, but rather by the tSZ effect from unresolved clusters. However the latter will contribute only at low redshifts when galaxy clusters have formed, whereas

the distortion from the non-linear kSZ effect due to the intergalactic medium, both in intensity and polarization, contributes mostly at the beginning of reionization around $z \simeq 12$, where the visibility function is the largest. This can be seen more rigorously by examination of the integrand of the Limber approximation [e.g. Eq. (3.10)] for the angular spectrum of polarization distortion E^y -modes. Once the Fourier modes integral has been performed, there remains only one integral on the comoving distance r , and by plotting the corresponding integrand in Fig. 4 for several multipoles, we find indeed that it is larger for high redshifts. The same result is found for the intensity y -type distortion spectrum. Apart from the very large angular scales,

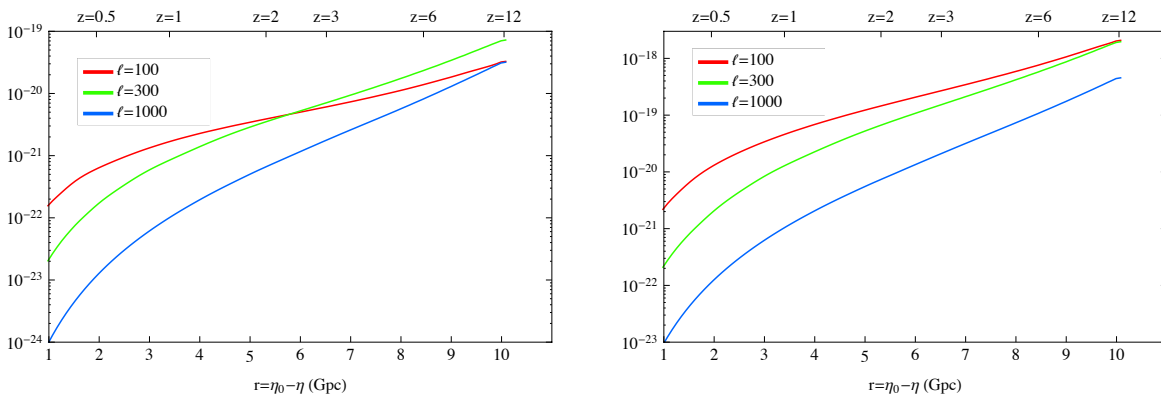


Figure 4. *Left.* From the Limber approximation (3.10) for the polarization distortion E^y -modes spectrum, we plot the integrand of the outer integral on the comoving distance r [multiplied by $\ell(\ell + 1)/(2\pi)$], for $\ell = 100$ (red), $\ell = 300$ (green) and $\ell = 1000$ (blue). *Right.* From the Limber approximation (C.16) for the intensity y -type distortion spectrum, we plot the integrand of the outer integral on the comoving distance r [multiplied by $\ell(\ell + 1)/(2\pi)$], for $\ell = 100$ (red), $\ell = 300$ (green) and $\ell = 1000$ (blue).

there would thus be no correlation between the tSZ signal and the intergalactic contribution to the non-linear kSZ effect. In Appendix C, we summarize the formalism necessary to compute the correlation between the y -type polarization distortion and the y -type intensity distortion. We have evaluated it numerically using SONG and plotted the results thus obtained in the right panel of Fig. 5. Unfortunately, it appears that the cross-correlation of the E^y -modes polarization distortion with the intensity distortion is actually not larger, but on the contrary slightly smaller in magnitude, than the auto correlation of the E^y -modes. However, to improve the detectability of our signal, correlating it with the y -type intensity distortion is not the only possibility. As we have mentioned in §. 2.2, the non-linear kSZ effect not only generates a spectral distortion component but also a similar contribution to the standard component $\mathcal{P}_{\mu\nu}$ of the polarization tensor. More precisely, the latter obeys an evolution equation similar to Eq. (2.11) in the tetrad basis, with a collision term containing 4 times the contribution (2.12). This second-order effect generates a correction to the standard E - and B -modes which is thus simply four times their spectrally distorted counterparts (2.20) and (2.21), leading to correlations $\langle E^{\text{st}} E^{y*} \rangle = 4 \langle E^y E^{y*} \rangle$ and $\langle B^{\text{st}} B^{y*} \rangle = 4 \langle B^y B^{y*} \rangle$ where st stands for the standard E - and B -modes (the leading order contributions to the latter do not correlate with the polarization distortion in a Gaussian universe,

as the corresponding correlation is proportional to the bispectrum of the primordial gravitational potential).

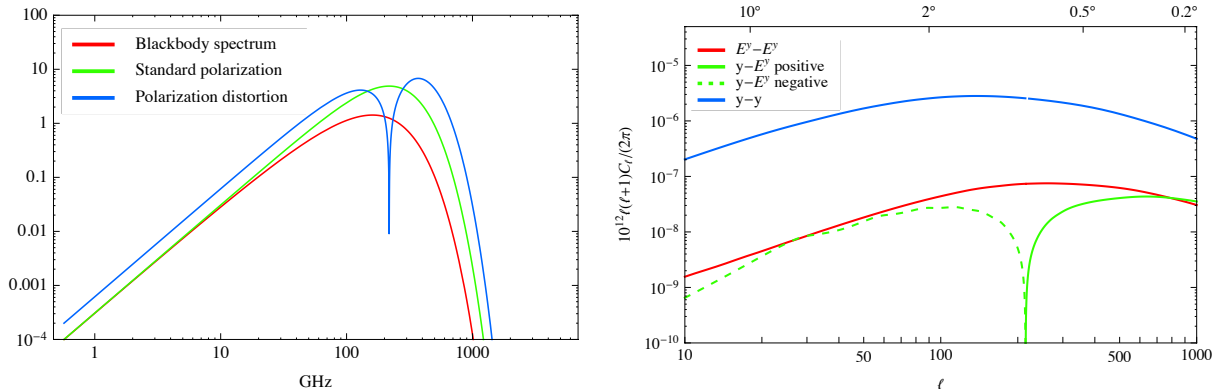


Figure 5. *Left.* Red: intensity brightness for a blackbody spectrum $[E^3 I_{\text{BB}}(E/T_0)]$. Green: brightness of the standard polarization $[E^3 \partial I_{\text{BB}}(E/T_0) / \partial \ln E]$. Blue: brightness of the y -type distortion $[E^3 \mathcal{D}_E^2 I_{\text{BB}}(E/T_0)]$ (see Eqs. (2.7) and (2.9)). All curves have been divided by T_0^3 to make them dimensionless, with $T_0 = 2.73$ K. The blackbody brightness peaks at 160 GHz, while the y -type distortion brightness peaks at 370 GHz. *Right.* Red: the angular power spectrum of polarization distortion E^y -modes; Green: the cross correlation of polarization distortion E^y -modes with y -type intensity distortion (continuous when positive and dashed when negative); Blue: the angular power spectrum of intensity y -type distortion.

Effects of an extended period of reionization The previous results were derived using a simple model of instantaneous reionization. In order to quantify to which extent a more realistic extended period of reionization modifies our signal, we consider the simple two-parameter model for the ionization history that is currently the default parameterization of the CAMB code [42, 43] and one of the two possible parameterizations of the CLASS code [44, 45]. In this model, the number of free electrons per hydrogen atom x_e is given by

$$x_e(z) \equiv \frac{n_e(z)}{n_H(z)} = \frac{f}{2} \left\{ 1 + \tanh \left[\frac{(1+z_r)^{3/2} - (1+z)^{3/2}}{\Delta} \right] \right\}, \quad (4.1)$$

where $f = 1 + n_{He}/n_H \sim 1.08$, z_r is the redshift at which the hydrogen is half neutral and ‘the duration of reionization’ Δ is the width of a tanh function that describes the time evolution of x_e . Note that the motivation for this simple model is merely mathematical: it is built such that the total optical depth is independent of Δ and thus coincides with the one of a model of instantaneous reionization, corresponding to the limit $\Delta \rightarrow 0$. In Fig. 6 we plot the modifications induced by an extended period of reionization corresponding to $\Delta = 1$ and $\Delta = 3$, together with the results for the reference instantaneous model, for the total E^y - and B^y -modes spectra (left), and for the y -type intensity distortion spectrum and its cross-correlation with the E^y -modes (right). From these plots, it is readily apparent that all these spectra are nearly insensitive

to the width of the reionization transition, the difference between the spectra corresponding to $\Delta = 0$ and $\Delta = 3$ being of 2% at the location of the peak (and nearly insensitive to the multipole ℓ). This shows that the physical processes studied in this paper constitute a probe of the total optical depth to reionization only.

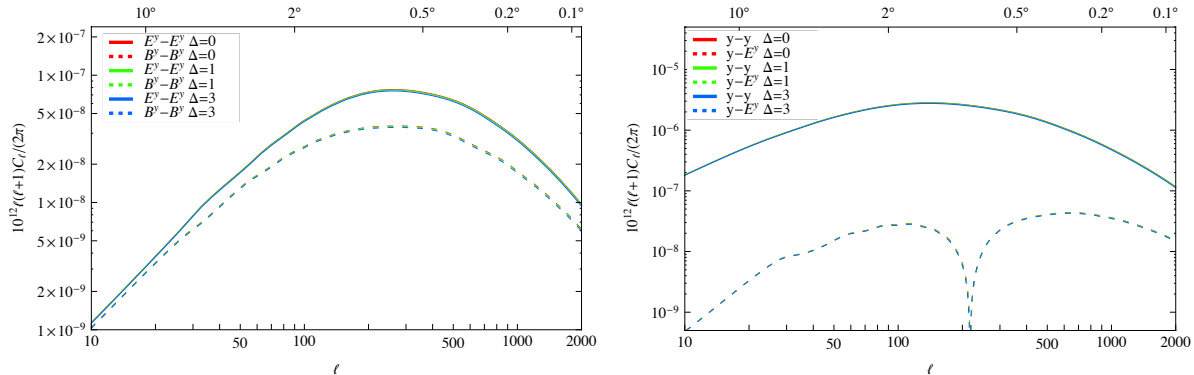


Figure 6. Effects of an extended period of reionization. *Left.* The total E^y -modes spectrum (continuous lines) and the total B^y -modes spectrum (dashed lines) for the model of instantaneous reionization (in red) and for the model of extended reionization (4.1) with the same value of z_r but with $\Delta = 1$ (green) and $\Delta = 3$ (blue). *Right.* The angular power spectrum of intensity y -type distortion (continuous lines) and the cross correlation of polarization distortion E^y -modes with y -type intensity distortion (dashed lines) for the model of instantaneous reionization (in red) and for the model of extended reionization (4.1) with the same value of z_r but with $\Delta = 1$ (green) and $\Delta = 3$ (blue).

5 Conclusions

CMB anisotropies measurements have now entered a high precision era in angular resolution. In addition, future CMB experiments aim to measure with great accuracy the deviation from blackbody nature of these anisotropies. This will open a new field of research and a new observational window into out-of-equilibrium and energy injection phenomena that cannot be probed otherwise, as well as it will add possibilities to set constraints on cosmological parameters. In particular, the angular correlations of temperature fluctuations, in two point function or higher order statistics, are not enough if we want to capture optimally the spectral information. Since CMB experiments measure both the intensity and the linear polarization, this spectral characterization has to be performed for both signals. Indeed, the main physical effect responsible for the spectral distortions of polarization is different from the one responsible for the intensity distortion. In the former case, the non-linear kSZ effect is the dominant contribution, whereas the thermal SZ effect dominates largely the intensity distortion. The cosmological information gathered from spectral distortions in polarization thus provides independent information.

In this article, we have computed the angular power spectrum of spectral distortions in polarization generated by the intergalactic medium. It is sourced by the difference between the velocities of electrons and photons, and its dominant contribution is therefore coming from the

epoch of reionization. Even though the signal is very small, it is guaranteed in the standard cosmological model, and since its spectral shape is very different from the one of the standard polarization of the CMB, it is in principle possible to disentangle them. Spectral distortions in polarization are mainly sensitive to the optical depth to reionization τ_{re} for which it could provide an independent estimation. Finally, we have found that most of the signal is on intermediary scales with an angular power spectrum which does not have baryon acoustic oscillation features. The numerical computation were performed with the second-order code **SONG** and we have shown that a Limber approximation is sufficient to compute the theoretical expectation of a given model for these scales of interest.

Acknowledgements

We would like to thank J.-P. Uzan and B. Wandelt for discussions related to the topic of this paper, as well as the anonymous referee whose useful comments helped us to improve it. This work was supported by French state funds managed by the ANR within the Investissements d’Avenir programme under reference ANR-11-IDEX-0004-02. G. Pettinari (respectively C. Fidler) acknowledges support from the UK Science and Technology Facilities Council grant number ST/I000976/1 (respectively grant numbers ST/K00090/1 and ST/L005573/1).

A Multipolar expansion of the collision term

In this appendix, we show how to obtain the multipolar expansion of

$$C_{ij}^{y(\text{L.O.})}(\mathbf{k}, \hat{\mathbf{n}}) = -\frac{1}{10} \mathcal{K} \{ [v_i(\mathbf{k}_1) v_j(\mathbf{k}_2)]^{\text{TT}} \} \quad (\text{A.1})$$

where we omit to mention the obvious time-dependence, and we recall that \mathcal{K} denotes the convolution operator (2.19). Writing

$$C_{ij}^{y(\text{L.O.})}(\mathbf{k}, \hat{\mathbf{n}}) = \sum_{\pm, \ell, m} \frac{1}{N_\ell} [E[C^y]_{\ell m}(\mathbf{k}) \pm iB[C^y]_{\ell m}(\mathbf{k})] Y_{\ell m}^{\pm 2}(\hat{\mathbf{n}}) m_i^\pm m_j^\pm, \quad (\text{A.2})$$

we can extract, using $m_i^\lambda m^{\lambda' i} = 1 - \delta^{\lambda, \lambda'}$ and $n^i m_i^\pm = 0$:

$$\sum_{\ell m} [E[C^y]_{\ell m}(\mathbf{k}) \pm iB[C^y]_{\ell m}(\mathbf{k})] \frac{Y_{\ell m}^{\pm 2}(\hat{\mathbf{n}})}{N_\ell} = -\frac{1}{10} \mathcal{K} \{ m^{\mp i} m^{\mp j} v_i(\mathbf{k}_1) v_j(\mathbf{k}_2) \}. \quad (\text{A.3})$$

Now, we use Eq. (2.16) to write

$$v_i(\mathbf{k}_1) n^i = \frac{1}{N_1} \sum_{m=-1}^1 Y_{1m}(\hat{\mathbf{n}}) v_m(\mathbf{k}_1) \quad (\text{A.4})$$

where

$$v_m(\mathbf{k}_1) = \sqrt{\frac{4\pi}{3}} Y_{1m}^*(\hat{\mathbf{k}}_1) F(k_1, \eta) \Phi(k_1) \quad (\text{A.5})$$

and where we recall that the spherical harmonics are defined with the z axis aligned along the direction of the Fourier vector \mathbf{k} of interest. Equipped with the projection Eq. (A.4) of v_i along the local normal vector n^i , we obtain its projection on the local polarization basis by differentiating this relation:

$$m^{\pm j} \nabla_j (v_i(\mathbf{k}_1) n^i) = v_i(\mathbf{k}_1) m^{\pm i}, \quad (\text{A.6})$$

where ∇_i is the covariant derivative on the unit-sphere. With

$$m^{\pm j} \nabla_j (Y_{1m}) = \pm Y_{1m}^{\mp 1}, \quad (\text{A.7})$$

we therefore obtain

$$m^{\mp i} m^{\mp j} v_i(\mathbf{k}_1) v_j(\mathbf{k}_2) = \frac{1}{N_1^2} \sum_{m,n} v_m(\mathbf{k}_1) v_n(\mathbf{k}_2) Y_{1m}^{\mp 1} Y_{1n}^{\mp 1} \quad (\text{A.8})$$

Noting eventually that

$$Y_{1m}^{\pm 1} Y_{1n}^{\pm 1} = \frac{3}{2\sqrt{5}\pi} \langle 1, m; 1, n | 2, m+n \rangle Y_{2, m+n}^{\pm 2}, \quad (\text{A.9})$$

where $\langle l_1, m_1; l_2, m_2 | l, m \rangle$ denotes the corresponding Clebsch-Gordan coefficient, we finally identify that $B[C^y]_{\ell m} = 0$ and

$$E[C^y]_{\ell m}(\mathbf{k}) = \delta_\ell^2 \mathcal{K} \left\{ S_m(\hat{\mathbf{k}}_1, \hat{\mathbf{k}}_2) F(k_1, \eta) F(k_2, \eta) \Phi(k_1) \Phi(k_2) \right\} \quad (\text{A.10})$$

where

$$S_m(\hat{\mathbf{k}}_1, \hat{\mathbf{k}}_2) = -\frac{\pi}{15} \sqrt{\frac{2}{3}} \sum_{n=-1}^1 \alpha_{n,m} \left(Y_1^{m-n}(\hat{\mathbf{k}}_1) Y_1^n(\hat{\mathbf{k}}_2) \right)^* \quad (\text{A.11})$$

with the notation

$$\alpha_{0,m} \equiv \sqrt{(4-m^2)}, \quad \alpha_{\pm 1,m} \equiv \sqrt{(2 \pm m)(2 \pm m - 1)/2} \quad (\text{A.12})$$

(this implies that $S_{-2} = S_2^*$ and $S_{-1} = -S_1^*$).

B Correlation functions of polarization patterns and angular power spectra

For the sake of completeness, in this appendix we give the relations between the angular power spectra calculated in section 3 and observable correlation functions. There is no original material here: these relations are formally the same as for the standard CMB polarization, and we refer the reader to Ref. [36] for instance, which we follow closely.

It is first convenient to define genuine spin-0 quantities out of the spin-2 Stokes parameters Q^y and U^y . We therefore define

$$\begin{aligned} \tilde{E}^y(\mathbf{x}, \mathbf{n}) &\equiv \frac{1}{2} [(\vartheta^*)^2 (Q^y + iU^y)(\mathbf{x}, \mathbf{n}) + \vartheta^2 (Q^y - iU^y)(\mathbf{x}, \mathbf{n})] \\ &= \sum_{\ell=2}^{\infty} \sum_{m=-\ell}^{\ell} \sqrt{\frac{(\ell+2)!}{(\ell-2)!}} e_{\ell m}^y(\mathbf{x}) Y_{\ell m}(\hat{\mathbf{n}}; \hat{\mathbf{e}}) \end{aligned} \quad (\text{B.1})$$

and

$$\begin{aligned}\tilde{B}^y(\mathbf{x}, \mathbf{n}) &\equiv -\frac{i}{2} [(\hat{\phi}^*)^2(Q^y + iU^y)(\mathbf{x}, \mathbf{n}) - \hat{\phi}^2(Q^y - iU^y)(\mathbf{x}, \mathbf{n})] \\ &= \sum_{\ell=2}^{\infty} \sum_{m=-\ell}^{\ell} \sqrt{\frac{(\ell+2)!}{(\ell-2)!}} b_{\ell m}^y(\mathbf{x}) Y_{\ell m}(\hat{\mathbf{n}}; \hat{\mathbf{e}}),\end{aligned}\tag{B.2}$$

where $\hat{\phi}$ and $\hat{\phi}^*$ are the spin raising and lowering operators and where $e_{\ell m}^y$ and $b_{\ell m}^y$ are defined in Eq. (3.2). Besides being spin-0 quantities, $\tilde{E}^y(\mathbf{x}, \mathbf{n})$ and $\tilde{B}^y(\mathbf{x}, \mathbf{n})$ are particularly convenient to adopt because they verify [36]

$$\tilde{E}^y = \text{div div } y_{ij}, \quad \tilde{B}^y = \text{rot rot } y_{ij}.\tag{B.3}$$

Hence \tilde{E}^y and \tilde{B}^y are locally related to the observable polarization distortion pattern y_{ij} and \tilde{E}^y measures ‘‘gradient-type’’ polarization distortion while \tilde{B}^y measures ‘‘curl-type’’ polarization distortion. They are directly related to the multipolar coefficients $E_{\ell m}^y$ and $B_{\ell m}^y$ as

$$\tilde{E}^y(\mathbf{x}, \mathbf{n}) = \int \frac{d^3\mathbf{k}}{(2\pi)^3} e^{i\mathbf{k}\cdot\mathbf{x}} \sum_{\ell=2}^{\infty} \sqrt{\frac{(\ell+2)!}{(\ell-2)!}} \sum_{m=-2}^2 E_{\ell m}^y(\mathbf{k}) Y_{\ell m}(\mathbf{n}; \mathbf{k})\tag{B.4}$$

$$\tilde{B}^y(\mathbf{x}, \mathbf{n}) = \int \frac{d^3\mathbf{k}}{(2\pi)^3} e^{i\mathbf{k}\cdot\mathbf{x}} \sum_{\ell=2}^{\infty} \sqrt{\frac{(\ell+2)!}{(\ell-2)!}} \sum_{m=-2}^2 B_{\ell m}^y(\mathbf{k}) Y_{\ell m}(\mathbf{n}; \mathbf{k})\tag{B.5}$$

where $Y_{\ell m}(\mathbf{n}; \mathbf{k})$ indicates that the spherical harmonics are defined with respect to the z axis aligned with the wave vector \mathbf{k} . We find therefore that their angular correlation functions are related to the power-spectra (3.3) by⁵

$$\langle \tilde{E}^y(\mathbf{x}, \mathbf{n}) \tilde{E}^y(\mathbf{x}, \mathbf{n}') \rangle = \frac{1}{4\pi} \sum_{\ell=0}^{\infty} \frac{(\ell+2)!}{(\ell-2)!} (2\ell+1) P_{\ell}(\mathbf{n} \cdot \mathbf{n}') C_{\ell}^{E^y}\tag{B.6}$$

$$\langle \tilde{B}^y(\mathbf{x}, \mathbf{n}) \tilde{B}^y(\mathbf{x}, \mathbf{n}') \rangle = \frac{1}{4\pi} \sum_{\ell=0}^{\infty} \frac{(\ell+2)!}{(\ell-2)!} (2\ell+1) P_{\ell}(\mathbf{n} \cdot \mathbf{n}') C_{\ell}^{B^y}\tag{B.7}$$

where P_{ℓ} denotes the Legendre polynomial of order ℓ .

C Cross-correlation with intensity distortion

In this appendix, we calculate the cross-correlation between the y -type polarization distortion and the y -type intensity distortion. Following the same reasoning as in the main text, we solve the Boltzmann equation for the intensity distortion

$$y' + n^i \partial_i y = \tau' (-y + C^y)\tag{C.1}$$

⁵There are typos in Eqs. 5.78-5.80 of Ref. [36], which are corrected here.

with the leading-order contribution to the collision term identified as [12]

$$C^y(\text{L.O.}) = \frac{1}{3}v_i v^i + \frac{11}{20}v_{\langle i} v_{j \rangle} n^i n^j, \quad (\text{C.2})$$

where $\langle ij \rangle$ means the symmetric traceless part. The corresponding integral solution is

$$y(\eta_0, k_i, n^i) = \int_{\eta_{\text{re}}}^{\eta_0} d\eta g(\eta) e^{-ik_i n^i r(\eta)} C^y(\text{L.O.})(\eta, k_i, n^i). \quad (\text{C.3})$$

We then expand in spherical harmonics the contribution of a given Fourier mode, for y :

$$y(\mathbf{k}, \hat{\mathbf{n}}) = \sum_{\ell=2}^{\infty} \sum_{m=-\ell}^{\ell} \frac{1}{N_\ell} y_{\ell m}(\mathbf{k}) Y_{\ell m}(\hat{\mathbf{n}}), \quad (\text{C.4})$$

and for the collision term:

$$C^y(\text{L.O.})(\eta, \mathbf{k}, \hat{\mathbf{n}}) = \sum_{\ell, m} \frac{1}{N_\ell} C_{\ell m}^y(\mathbf{k}) Y_{\ell m}(\hat{\mathbf{n}}). \quad (\text{C.5})$$

Following steps similar to the ones detailed in Appendix A, we find a monopolar and a quadrupolar contribution:

$$C_{\ell m}^y = \mathcal{K} \left\{ \left[\delta_\ell^0 \delta_m^0 S_{00}^y(\hat{\mathbf{k}}_1, \hat{\mathbf{k}}_2) + \delta_\ell^2 S_{2m}^y(\hat{\mathbf{k}}_1, \hat{\mathbf{k}}_2) \right] F(k_1, \eta) F(k_2, \eta) \Phi(k_1) \Phi(k_2) \right\} \quad (\text{C.6})$$

where

$$S_{00}^y(\hat{\mathbf{k}}_1, \hat{\mathbf{k}}_2) = -\frac{1}{3} \hat{\mathbf{k}}_1 \cdot \hat{\mathbf{k}}_2 \quad (\text{C.7})$$

and

$$S_{2m}^y(\hat{\mathbf{k}}_1, \hat{\mathbf{k}}_2) = -\frac{11}{\sqrt{6}} S_m(\hat{\mathbf{k}}_1, \hat{\mathbf{k}}_2) = \frac{11\pi}{45} \sum_{n=-1}^1 \alpha_{n,m} \left(Y_1^{m-n}(\hat{\mathbf{k}}_1) Y_1^n(\hat{\mathbf{k}}_2) \right)^*. \quad (\text{C.8})$$

Using the Rayleigh formula, we then obtain

$$\frac{y_{\ell m}(\mathbf{k})}{2\ell + 1} = \mathcal{K} \left\{ \int_{\eta_{\text{re}}}^{\eta_0} d\eta g(\eta) \left[j_\ell \delta_m^0 S_{00}^y(\hat{\mathbf{k}}_1, \hat{\mathbf{k}}_2) + j_\ell^{(2m)} [kr(\eta)] S_{2m}^y(\hat{\mathbf{k}}_1, \hat{\mathbf{k}}_2) \right] F(k_1, \eta) F(k_2, \eta) \Phi(k_1) \Phi(k_2) \right\} \quad (\text{C.9})$$

where the expressions of the functions $j_\ell^{(2m)}$ are given in Appendix D. From this the angular power spectra can be obtained by summing all the Fourier modes contributions, giving

$$(2\ell + 1)^2 C_\ell^{y E^y} = \frac{2}{\pi} \sum_{m=-2}^2 \int dk k^2 \mathcal{Q}_{\ell m}^{y E^y}(k) \quad (\text{C.10})$$

$$(2\ell + 1)^2 C_\ell^y = \frac{2}{\pi} \sum_{m=-2}^2 \int dk k^2 \mathcal{Q}_{\ell m}^{yy}(k) \quad (\text{C.11})$$

(the correlation between y and B^y vanishes by parity), where we defined

$$\langle y_{\ell m}(\mathbf{k}) E_{\ell m'}^{y*}(\mathbf{k}') \rangle = (2\pi)^3 \delta^3(\mathbf{k} - \mathbf{k}') \mathcal{Q}_{\ell m}^{y E^y}(k) \delta_{mm'} \quad (\text{C.12})$$

$$\langle y_{\ell m}(\mathbf{k}) y_{\ell m'}(\mathbf{k}') \rangle = (2\pi)^3 \delta^3(\mathbf{k} - \mathbf{k}') \mathcal{Q}_{\ell m}^{yy}(k) \delta_{mm'} . \quad (\text{C.13})$$

From Eqs. (2.20)-(C.9), one easily obtains

$$\mathcal{Q}_{\ell m}^{yy}(k) = \frac{2(2\ell + 1)^2}{(2\pi)^3} \int d^3 \mathbf{k}_1 P(k_1) P(k_2) \quad (\text{C.14})$$

$$\left| \int_{\eta_{\text{re}}}^{\eta_0} d\eta g(\eta) \left\{ S_{2m}^y(\hat{\mathbf{k}}_1, \hat{\mathbf{k}}_2) j_\ell^{(2m)}[kr(\eta)] + S_{00}^y(\hat{\mathbf{k}}_1, \hat{\mathbf{k}}_2) j_\ell[kr(\eta)] \delta_m^0 \right\} F(k_1, \eta) F(k_2, \eta) \right|^2$$

and

$$\begin{aligned} \mathcal{Q}_{\ell m}^{y E^y}(k) &= \frac{2(2\ell + 1)^2}{(2\pi)^3} \int d^3 \mathbf{k}_1 P(k_1) P(k_2) \\ &\times \left(\int_{\eta_{\text{re}}}^{\eta_0} d\eta g(\eta) \left\{ S_{2m}^y(\hat{\mathbf{k}}_1, \hat{\mathbf{k}}_2) j_\ell^{(2m)}[kr(\eta)] + S_{00}^y(\hat{\mathbf{k}}_1, \hat{\mathbf{k}}_2) j_\ell[kr(\eta)] \delta_m^0 \right\} F(k_1, \eta) F(k_2, \eta) \right) \\ &\times \left(S_m^*(\hat{\mathbf{k}}_1, \hat{\mathbf{k}}_2) \int_{\eta_{\text{re}}}^{\eta_0} d\eta g(\eta) \epsilon_\ell^{(m)}[kr(\eta)] F(k_1, \eta) F(k_2, \eta) \right) , \end{aligned} \quad (\text{C.15})$$

with the same notations as in § 3.2. Following the same arguments as there, we find that the auto-correlation of intensity distortion reads, within the Limber approximation:

$$\begin{aligned} C_{\ell}^y \text{Limber} &= \frac{2}{(2\pi)^2} \int_0^{r_{\text{re}}} \frac{dr}{r^2} k_1^2 dk_1 \sin \theta_{\mathbf{k}_1} d\theta_{\mathbf{k}_1} P(k_1) P(k_2) (g(\eta) F(k_1, \eta) F(k_2, \eta))^2 \\ &\times \left(\left| S_{00}^y(\hat{\mathbf{k}}_1, \hat{\mathbf{k}}_2) + \frac{1}{2} S_{20}^y(\hat{\mathbf{k}}_1, \hat{\mathbf{k}}_2) \right|^2 + \frac{3}{4} \left| S_{22}^y(\hat{\mathbf{k}}_1, \hat{\mathbf{k}}_2) \right|^2 \right) . \end{aligned} \quad (\text{C.16})$$

Similarly, the cross correlation between intensity distortion and polarization distortion is, in the Limber approximation:

$$\begin{aligned} C_{\ell}^{y E^y} \text{Limber} &= \frac{2}{(2\pi)^2} \int_0^{r_{\text{re}}} \frac{dr}{r^2} k_1^2 dk_1 \sin \theta_{\mathbf{k}_1} d\theta_{\mathbf{k}_1} P(k_1) P(k_2) (g(\eta) F(k_1, \eta) F(k_2, \eta))^2 \\ &\times \left\{ \sqrt{\frac{3}{8}} \left[S_{00}^y(\hat{\mathbf{k}}_1, \hat{\mathbf{k}}_2) + \frac{1}{2} S_{20}^y(\hat{\mathbf{k}}_1, \hat{\mathbf{k}}_2) \right] S_0^*(\hat{\mathbf{k}}_1, \hat{\mathbf{k}}_2) - \frac{1}{4} \sqrt{\frac{3}{2}} S_{22}^y(\hat{\mathbf{k}}_1, \hat{\mathbf{k}}_2) S_2^*(\hat{\mathbf{k}}_1, \hat{\mathbf{k}}_2) \right\} . \end{aligned} \quad (\text{C.17})$$

It is displayed on the right panel of Fig. 5.

D Expressions of special functions

We first give the expressions of $\epsilon_\ell^{(m)}$ and $\beta_\ell^{(m)}$ entering into the results Eqs. (2.20)-(2.21) for the spectral distortions E - and B -modes:

$$\begin{aligned}\epsilon_\ell^{(0)}(x) &= \sqrt{\frac{3}{8} \frac{(\ell+2)!}{(\ell-2)!} \frac{j_\ell(x)}{x^2}}, \\ \epsilon_\ell^{(1)}(x) &= \frac{1}{2} \sqrt{(\ell-1)(\ell+2)} \left[\frac{j_\ell(x)}{x^2} + \frac{j'_\ell(x)}{x} \right], \\ \epsilon_\ell^{(2)}(x) &= \frac{1}{4} \left[-j_\ell(x) + j''_\ell(x) + 2 \frac{j_\ell(x)}{x^2} + 4 \frac{j'_\ell(x)}{x} \right]\end{aligned}\tag{D.1}$$

and

$$\begin{aligned}\beta_\ell^{(0)}(x) &= 0, \\ \beta_\ell^{(1)}(x) &= \frac{1}{2} \sqrt{(\ell-1)(\ell+2)} \frac{j_\ell(x)}{x}, \\ \beta_\ell^{(2)}(x) &= \frac{1}{2} \left[j'_\ell(x) + 2 \frac{j_\ell(x)}{x} \right],\end{aligned}\tag{D.2}$$

where $j_\ell(x)$ denotes the spherical Bessel function of order ℓ , and with $\epsilon_\ell^{(-1)} = \epsilon_\ell^{(1)}$, $\epsilon_\ell^{(-2)} = \epsilon_\ell^{(2)}$, $\beta_\ell^{(-1)} = -\beta_\ell^{(1)}$ and $\beta_\ell^{(-2)} = -\beta_\ell^{(2)}$.

We then give the expressions of $j_\ell^{(2m)}$ entering into the result Eq. (C.9) for the intensity spectral distortion:

$$j_\ell^{(20)}(x) = \frac{1}{2} [3j''_\ell(x) + j_\ell(x)],\tag{D.3}$$

$$j_\ell^{(21)}(x) = \sqrt{\frac{3\ell(\ell+1)}{2}} \left(\frac{j_\ell(x)}{x} \right)',\tag{D.4}$$

$$j_\ell^{(22)}(x) = \sqrt{\frac{3}{8} \frac{(\ell+2)!}{(\ell-2)!} \frac{j_\ell(x)}{x^2}},\tag{D.5}$$

with $j_\ell^{(2-2)} = j_\ell^{(22)}$ and $j_\ell^{(2-1)} = j_\ell^{(21)}$.

References

- [1] P. A. R. Ade *et al.* [Planck Collaboration], arXiv:1303.5076 [astro-ph.CO].
- [2] A. Lewis and A. Challinor, Phys. Rept. **429** (2006) 1 [astro-ph/0601594].
- [3] P. A. R. Ade *et al.* [Planck Collaboration], arXiv:1303.5077 [astro-ph.CO].

- [4] P. A. R. Ade *et al.* [Planck Collaboration], [arXiv:1303.5084 [astro-ph.CO]].
- [5] P. Andre *et al.* [PRISM Collaboration], [arXiv:1306.2259 [astro-ph.CO]].
- [6] A. Kogut, D. J. Fixsen, D. T. Chuss, J. Dotson, E. Dwek, M. Halpern, G. F. Hinshaw and S. M. Meyer *et al.*, JCAP **1107** (2011) 025 [arXiv:1105.2044 [astro-ph.CO]].
- [7] Ya. B. Zel'dovich and R.A. Sunyaev, Astrophys. Sp. Sci. **4** 301 (1969).
- [8] R. A. Sunyaev and R. Khatri, Int. J. Mod. Phys. D **22** (2013) 1330014 [arXiv:1302.6553 [astro-ph.CO]].
- [9] J. Chluba and R. A. Sunyaev, [arXiv:1109.6552 [astro-ph.CO]].
- [10] J. Chluba, R. Khatri and R. A. Sunyaev, [arXiv:1202.0057 [astro-ph.CO]].
- [11] A. Stebbins, [astro-ph/0703541].
- [12] C. Pitrou, F. Bernardeau and J.-P. Uzan, JCAP **1007** (2010) 019 [arXiv:0912.3655 [astro-ph.CO]].
- [13] P. A. R. Ade *et al.* [Planck Collaboration], [arXiv:1303.5081 [astro-ph.CO]].
- [14] A. Challinor, M. Ford and A. Lasenby, Mon. Not. Roy. Astron. Soc. **312** (2000) 159 [astro-ph/9905227].
- [15] W. Hu, Astrophys. J. **529** (2000) 12 [astro-ph/9907103].
- [16] G. Lavaux, J. M. Diego, H. Mathis and J. Silk, Mon. Not. Roy. Astron. Soc. **347** (2004) 729 [astro-ph/0307293].
- [17] D. Baumann, A. Cooray and M. Kamionkowski, New Astron. **8** (2003) 565 [astro-ph/0208511].
- [18] R. A. Sunyaev and Y. B. Zeldovich, MNRAS **190** (1980) 413.
- [19] S. Y. Sazonov and R. A. Sunyaev, MNRAS **310** (1999) 765 [astro-ph/9903287].
- [20] A. Naruko, C. Pitrou, K. Koyama and M. Sasaki, [arXiv:1304.6929 [astro-ph.CO]].
- [21] C. Pitrou, Class. Quant. Grav. **26** (2009) 065006 [arXiv:0809.3036 [gr-qc]].
- [22] M. Beneke and C. Fidler, Phys. Rev. D **82** (2010) 063509 [arXiv:1003.1834 [astro-ph.CO]].
- [23] C. G. Tsagas, A. Challinor and R. Maartens, Phys. Rept. **465** (2008) 61 [arXiv:0705.4397 [astro-ph]].
- [24] S. Dodelson. *Modern cosmology*, Academic Press (2003).
- [25] S. Dodelson and J. M. Jubas. Astrophys. J. **439** (1995) 503 [astro-ph/9308019].
- [26] W. Hu, D. Scott, and J. Silk. Phys. Rev. D **49** (1994) 648 [astro-ph/9305038].
- [27] U. Seljak and M. Zaldarriaga, Phys. Rev. Lett. **78** (1997) 2054 [astro-ph/9609169].
- [28] C. Pitrou and A. Stebbins, [arXiv:1402.0968 [astro-ph.CO]].
- [29] W. Hu, Phys. Rev. D **62** (2000) 043007 [astro-ph/0001303].
- [30] P. J. E. Peebles and J. T. Yu, Astrophys. J. **162** (1970) 815.
- [31] C. -P. Ma and E. Bertschinger, Astrophys. J. **455** (1995) 7 [astro-ph/9506072].
- [32] C. Pitrou, Phys. Lett. B **698** (2011) 1 [arXiv:1012.0546 [astro-ph.CO]].
- [33] F. -Y. Cyr-Racine and K. Sigurdson, Phys. Rev. D **83** (2011) 103521 [arXiv:1012.0569]

- [astro-ph.CO]].
- [34] U. Seljak and M. Zaldarriaga, *Astrophys. J.* **469** (1996) 437 [astro-ph/9603033].
 - [35] W. Hu and M. White, *Phys. Rev. D* **56** (1997) 596 [astro-ph/9702170].
 - [36] R. Durrer, *The Cosmic Microwave Background*, Cambridge University Press (2008).
 - [37] D. N. Limber, *Astrophys. J.* **117** 134 (1953).
 - [38] F. Bernardeau, C. Pitrou and J.-P. Uzan, *JCAP* **1102** (2011) 015 [arXiv:1012.2652 [astro-ph.CO]].
 - [39] M. LoVerde and N. Afshordi, *Phys. Rev. D* **78** (2008) 123506 [arXiv:0809.5112 [astro-ph]].
 - [40] G. W. Pettinari, C. Fidler, R. Crittenden, K. Koyama and D. Wands, *JCAP* **1304** (2013) 003 [arXiv:1302.0832 [astro-ph.CO]].
 - [41] C. Fidler, G. W. Pettinari, M. Beneke, *et al* (2014) [arXiv:1401.3296 [astro-ph.CO]]
 - [42] A. Lewis, A. Challinor and A. Lasenby, *Astrophys. J.* **538** (2000) 473 [astro-ph/9911177].
 - [43] A. Lewis, *Phys. Rev. D* **78** (2008) 023002 [arXiv:0804.3865 [astro-ph]].
 - [44] <http://class-code.net>
 - [45] D. Blas, J. Lesgourgues and T. Tram, *JCAP* **1107** (2011) 034 [arXiv:1104.2933 [astro-ph.CO]].